Applied Surface Science 566 (2021) 150662

Contents lists available at ScienceDirect

Applied Surface Science

journal homepage: www.elsevier.com/locate/apsusc

Full Length Article

Facet-dependent activity of tailored anatase TiO_2 crystals in photoanodes for photocatalytic fuel cells

Paweł Mikrut [a], Dariusz Mitoraj [b], Radim Beranek [b], Wojciech Macyk [a,*]

[a] Faculty of Chemistry, Jagiellonian University in Kraków, ul. Gronostajowa 2, 30-387 Kraków, Poland
[b] Institute of Electrochemistry, Ulm University, Albert-Einstein-Allee 47, 89081 Ulm, Germany

ARTICLE INFO

Keywords:
Photocatalytic fuel cells
Tailored crystals
Titanium dioxide
Photoelectrochemistry

ABSTRACT

A key component of the photocatalytic fuel cell (PFC) is a photoanode, typically based on highly stable semiconductor (*e.g.*, TiO_2) that is capable of effective photoelectrocatalytic oxidation of fuels. Notably, the photo (electro)catalytic activity of TiO_2 materials can depend heavily on the microstructural morphology, so that tailored crystals with different shapes and exposed facets can show remarkably different, shape-dependent photoactivities. Herein, we study the PFC performance of photoanodes based on anatase crystals of various shapes – tetragonal truncated bipyramids, sheets and belts, which are characterized by different predominantly exposed facets: {101}, {001}, and {100}, respectively. We demonstrate that photoanodes based on belt-shaped crystals dominated by {100} facets, not observed in natural anatase crystals, exhibit superior performance. Analysis of open-circuit potential and impedance data suggests that this activity is related to faster transfer of photogenerated holes to methanol oxidation sites, avoiding thus the undesired surface trapping and Fermi level pinning effects that are the most likely reason of a poorer performance of materials dominated by {101} and {001} facets. This study highlights the importance of advanced crystal engineering and control over the surface catalytic properties of TiO_2 materials for PFCs and other light-driven devices in which efficient alcohol photooxidation is crucial.

1. Introduction

The demand for electricity is growing every year, along with this, a significant increase in greenhouse gas emissions and air pollution associated with production of electricity is observed. These problems stimulate development of methods for the production, conversion and storage of electric energy based on renewable resources to reduce the consumption of fossil fuels. Among other approaches, conversion of chemical energy into electrical energy in fuel cells is a clean technology which can utilize either solar fuels (*e.g.*, hydrogen or alcohols from water splitting and CO_2 reduction) or processed biomass. One of the examples of such approach is a direct-alcohol fuel cell [1]. Compared to the most common hydrogen-based fuel cells, cells using liquid fuels like alcohols offer several advantages, such as uncomplicated storage and an easy availability from biomass and/or solar fuel producing systems. However, the direct-alcohol fuel cells (*e.g.*, methanol fuel cells that have a theoretical cell voltage of 1.20 V at 25 °C, hence comparable to H_2/O_2 cells) are typically hampered by very sluggish kinetics of alcohol oxidation at room temperature. This limitation can be possibly overcome using the concept of a *photocatalytic fuel cell* (PFC) in which photo(electro)catalysis is leveraged to circumvent the high activation barrier for dark alcohol oxidation at room temperature and the produced electrical energy results from transformation of both photon energy (light) and chemical energy of fuels (*e.g.*, alcohols, sugars, carboxylic acids) [2–5]. Therefore, PFC combines a functionality of a photovoltaic device with a fuel cell. Moreover, PFC technology allows to recover the chemical energy stored in wastewater by degradation of pollutants, and generation of electricity simultaneously [6–8]. For the development of PFC technology, suitable and inexpensive photoanode materials to produce electricity with a high efficiency are highly desirable. PFCs containing commercially available TiO_2 as a photoanode material were studied quite extensively [9,10], due to high activity of titania in photocatalyzing oxidation of organics. Moreover, metal supported anode photocatalysts were investigated, *e.g.,* Ag-TiO_2 [6,11], Pt-TiO_2 [12], Pt-Ru-TiO_2 [13], TiO_2/Ti [14], as well as composite materials, *e.g.,* CdS/TiO_2 [15] and CdS/ZnS/TiO_2 [7,16].

Notably, the photo(electro)catalytic activity of TiO_2 materials can depend heavily on the microstructural morphology, so that tailored

* Corresponding author.
E-mail address: macyk@chemia.uj.edu.pl (W. Macyk).

https://doi.org/10.1016/j.apsusc.2021.150662
Received 27 May 2021; Received in revised form 12 July 2021; Accepted 13 July 2021
Available online 17 July 2021

crystals with different shapes (*e.g.*, nanorods) [15,17–19] and different amounts of various facets can show remarkably different, shape-dependent photoactivities [11,20–22], compared to more commonly used, non-tailored materials. In our previous work, we showed that changing the shape of anatase TiO_2 crystals leads to significant changes of redox and light absorption properties of these materials [23]. It is widely accepted that due to the differences in the energy position of the conduction and valence band edges of different facets upon Fermi level alignment, a surface junction within a single TiO_2 crystal can be formed [24,25]. This can lead to an enhanced electron-hole separation as the {1 0 1} and {0 0 1} facets act as sinks of electrons and holes, respectively [20–22,26], leading thus to increased photoactivity. Nevertheless, the shape-dependent activity of tailored crystals is sometimes also explained by preferential selective adsorption of reactants and specific redox catalytic properties of different planes, rather than by intrinsically facet-selective separation of the photogenerated charges [27–29]. Various exposed anatase facets possess different atomic arrangements, *i.e.*, various densities of undercoordinated Ti_{5C} surface atoms and different Ti-O-Ti bond angles. For example, either 100% or 50% of titanium atoms exist as Ti_{5C} on {0 0 1} and {1 0 1} facets, respectively. Moreover, the Ti-O-Ti angle at {0 0 1} facets is 146°, in contrast to 102° in the case of {1 0 1} facets. It has been, for example, sometimes suggested that facets with a higher number of undercoordinated Ti atoms and a larger Ti-O-Ti angle, such as {0 0 1} facets, exhibit a better photocatalytic activity [30,31]. Moreover, owing to various atomic arrangements at different exposed facets, the adsorption of various reactants differs at different TiO_2 crystal planes. For example, simple chain alcohols can be adsorbed molecularly or dissociatively at {1 0 1} and {0 0 1} crystal facets, respectively [32–34]. Although tailored TiO_2 crystals have been studied extensively in the context of their photocatalytic activity, only one scientific report describing tailored crystals as a photoanode material in PFC is available so far [35]. Khalil et al. investigated the role of co-exposed {0 0 1} and {1 0 1} facets on the performance of $TiO_2/BiVO_4$ composite photoanodes, and reported the highest electric power generation (with Rhodamine B dye used as a fuel) for photoanodes based on truncated octahedra exposing predominantly {1 0 1} crystals facets [35]. In our previous work, we demonstrated a strong dependence of photocurrents in the presence of methanol on the crystal shape, whereby the most efficient photocurrent generation was observed for crystals with predominant {0 0 1} facets [23]. Several other studies also suggested an improved alcohol oxidation for crystals with exposed {0 0 1} facets compared to commercial materials or crystals offering other facets [36–38]. These rather scarce and partially conflicting reports exemplify that our knowledge of the effects of the shape and exposed facets of TiO_2 anatase crystals on current generation *via* photoelectrocatalytic alcohol oxidation is still significantly underdeveloped. In this work, therefore, we study the performance of photoanodes based on anatase crystals of various shapes – tetragonal truncated bipyramids, sheets and belts, which are characterized by different predominantly exposed facets: {1 0 1}, {0 0 1}, and {1 0 0}, respectively. We demonstrate that photoanodes based on belt-shaped crystals dominated by {1 0 0} facets exhibit superior performance, and discuss the importance of our findings for further development of PFC technology.

2. Experimental section

2.1. Synthesis of tailored crystals

The synthesis of anatase crystals was carried out using commercially available reagents. All chemicals used in this work were of analytical grade and were used as received. In order to synthesize tailored anatase crystals, the hydrothermal synthesis was applied. For synthesis of tetragonal truncated bipyramids and sheets-like crystals, titanium tetrachloride ($TiCl_4$, 98%, Fluka) and sodium fluoride (NaF, 97% Acros Organics) were used as the precursor and capping agent, respectively. Belts-like crystals were synthesized using a hydrothermal method that involved a consecutive formation of $Na_2Ti_3O_7$, $H_2Ti_3O_7$ and TiO_2 phases as the result of the ion exchange and calcination. Detailed information on the synthesis was published recently [23]. For the sake of clarity, TiO_2 materials composed of tetragonal truncated bipyramids, belts and sheets are abbreviated as **101**, **100** and **001**, respectively.

2.2. Photoanode preparation

Fluorine-doped tin oxide (FTO)-coated glass plates (2.5 × 1.5 cm^2, Pilkington TEC 15) were cleaned by sonication in acetone for 15 min, followed by boiling in 0.1 M NaOH for 5 min and rinsing with deionized water. The synthesized photocatalyst powder suspension in ethanol was sonicated for 15 min and then smeared on to the FTO glass. Subsequently, electrodes were dried in air, pressed for 1 min at the pressure of 50 kg/cm^2, and sintered at 450 °C for 0.5 h in order to ensure a good electrical contact.

2.3. Crystal structure and photoanode morphology

The phase compositions of synthesized materials were studied by the powder X-ray diffraction (XRD) using a Rigaku MiniFlex 600 X-ray diffractometer (Cu K_α radiation, 0.3 mm filter) in a 2θ degree range from 10° to 90°, speed 3°/min and 0.05° step.

The photoanodes morphology was examined by the scanning electron microscope (SEM) VEGA 3 TESCAN with an LaB_6 cathode. The measurements were performed on FTO glass without gold sputtering.

2.4. Photoelectrochemical measurements and fuel cell characterization

Photocurrent measurements were performed using the three-electrode setup with a platinum counter electrode and an Ag/AgCl (3 M KCl) reference electrode. During photocurrent measurements the cell was controlled using a SP-300 BioLogic potentiostat. All potential values are reported versus the reversible hydrogen electrode (RHE). Electrodes were irradiated (irradiation area 0.5 cm^2) from the backside (through the FTO glass) using a 150 W xenon lamp (LOT Oriel). The xenon lamp was equipped with the KG-3 (LOT GmbH) heat absorber, as well as with the AM 1.5G filter (irradiation power: 107 mW/cm^2; 1.07 sun). Photocurrents were recorded under intermittent irradiation (5 s light, 5 s dark) in various electrolytes and pH conditions: pH 5: 0.1 M boric acid; pH 7: phosphate buffer; pH 9: borate buffer; pH 13: 0.1 M KOH. Transient photocurrents were recorded in 0.1 M KOH (pH 13) in a three-electrode setup at 1.0 V *vs*. RHE using an Autolab PGSTAT302N potentiostat. A 375 nm LED was used as the light source (2.23 mW/cm^2).

A two-electrode system was used to study the PFC performance. The current–voltage (J-V) characteristics of the PFC system were obtained using the SP-300 BioLogic potentiostat. Electrodes were irradiated (irradiation area of the photoanode was 0.5 cm^2) from the backside using the same system (light source and filter) as mentioned before. The measured current and voltage values were used to calculate the generated electric power per unit area of the photoanode. All the PFC performance tests were carried out at room temperature in the presence of air in a home-made cell with a scan rate of 5 mV/s. Moreover, various pH conditions as well as various alcohols as fuels were tested. The long-term performances (discharging performances) of the fuel cells operation at a constant discharging current density of 20 μA/cm^2 in 0.1 M KOH with 5% (w/w) methanol were investigated. The fill factor (FF) was calculated as $FF = P_{MAX}/(V_{OC} \times J_{SC})$, in which P_{MAX} is the maximum power output under 1.07 sun solar irradiation, while V_{OC} and J_{SC} are the open circuit voltage and short circuit current, respectively.

Electrochemical impedance spectroscopy (EIS) measurements were performed at the AC voltage amplitude of 10 mV and the frequency range of 0.1 Hz to 100 kHz at V_{OC} potential in the presence/absence of methanol (5% w/w) upon irradiation (AM 1.5G; irradiation power: 107 mW/cm^2).

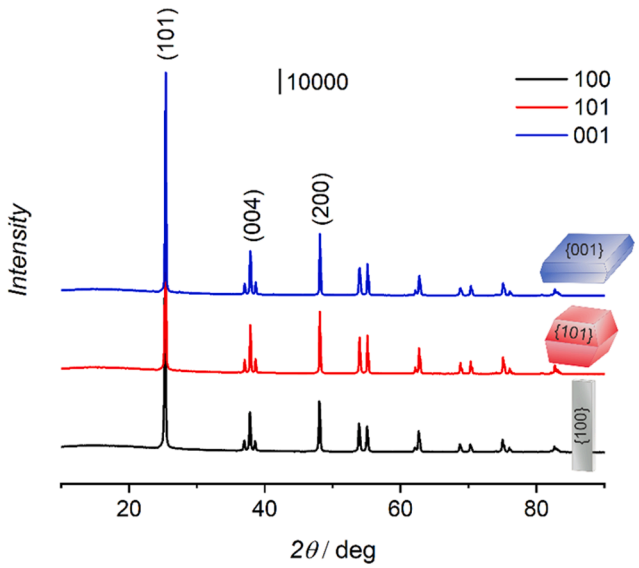

Fig. 1. XRD patterns of synthesized tailored TiO_2 crystals.

3. Results and discussion

3.1. Crystal structure and photoanode morphology

All synthesized materials were obtained in the form of white powders. The crystal structure and phase purity were determined using X-ray diffraction. The XRD patterns of all three tailored TiO_2 materials (Fig. 1) show exclusively the presence of the anatase phase. The differences in the signal intensity ratios result from different exposition of various crystallographic planes in the obtained crystals, which is in agreement with the corresponding crystal shapes. A more detailed material characterization is presented elsewhere [23].

The photoanode morphology and crystal shape were also examined by the SEM (Fig. 2). A high quality of photoanode is crucial to provide an efficient electron transport and thereby a high current density. The good quality of the semiconductor films on FTO support, as well as well-developed shapes of tailored crystals, were confirmed by SEM. SEM images show also a uniform coverage of photoanodes by TiO_2 crystals. The thickness of TiO_2 layers on the FTO support was in the range of *ca.* 1.4 to 2.1 μm, as concluded from SEM cross-sections of the films.

3.2. Photoelectrochemical measurements

Photoelectrochemical performance of prepared photoanodes was studied under simulated solar irradiation. The photoanodes were irradiated from the backside (through the FTO glass) since, compared to the frontside illumination, the backside irradiation led to higher photocurrents, as expected for photoanodes with porous morphology [39,40]. In order to study the electrolyte effects, the measurements were carried out in various electrolytes at different pH values. Furthermore, all photoanodes were tested with and without methanol (5% w/w) to compare the influence of exposed facets on the efficiency of photocurrent generation in the presence and absence of an additional electron donor, respectively. Photocurrents generated (at the same bias with respect to the reversible hydrogen electrode, RHE) by the studied photoanodes increased with increasing pH of the electrolyte (see Supporting Information, Fig. S1). The highest photocurrent densities measured at pH = 13 amounted to 0.101, 0.077, and 0.040 mA/cm^2 at 1.0 V *vs.* RHE for the **100**, **001** and **101** materials, respectively (Fig. 3a). In the presence of methanol, the highest photocurrent densities, at the same potential and pH, increased to 0.170, 0.097, and 0.047 mA/cm^2, respectively (Fig. 3b). Accordingly, the photocurrent multiplication factors for studied photoanodes amounted therefore to 1.68 (**100**), 1.26 (**001**) and 1.17 (**101**). A relatively better photoelectrochemical performance in alkaline electrolyte can be attributed to more effective scavenging of protons produced during oxidation reactions. Increased photocurrent generation in the presence of methanol is the result of the faster kinetics of alcohol oxidation as compared to oxidation of water, as well as of the formation of intermediate hydroxymethyl radical species that can inject an additional electron into the conduction band of TiO_2 ("photocurrent doubling" effect) [41,42]. Further photocatalytic fuel cell performance studies presented below were performed at pH = 13.

Photocurrent transients recorded in the *absence* of methanol exhibit, most notably in the case of **001** and **100** materials, a typical spike-like behaviour that is characteristic of intense surface recombination

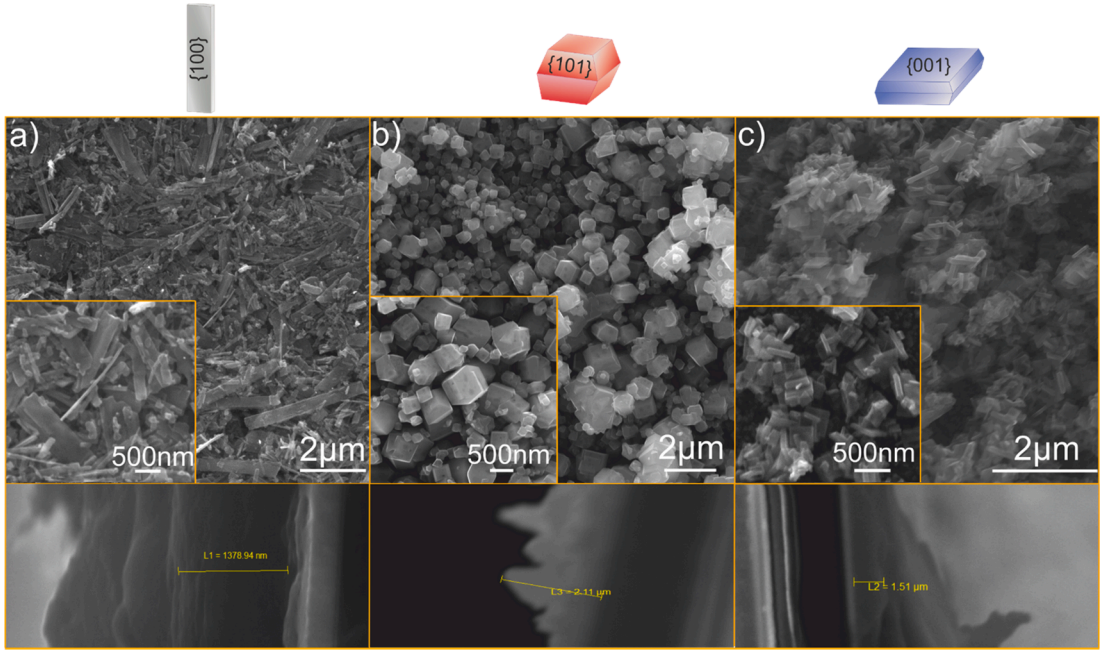

Fig. 2. SEM images of photoanodes made of TiO_2 crystals in the shape of a) belts (**100**), b) tetragonal truncated bipyramids (**101**) and c) sheets (**001**).

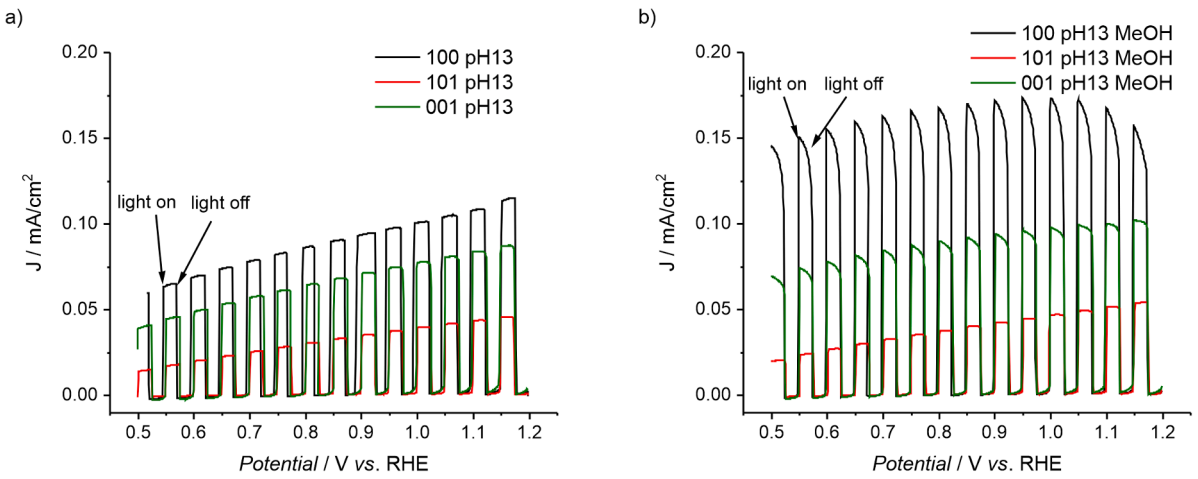

Fig. 3. Photocurrents measured at electrodes made of various tailored TiO_2 crystals under polychromatic irradiation (AM 1.5G; 1.07 sun) at pH = 13 in the absence (a) and presence (b) of methanol 5% (w/w).

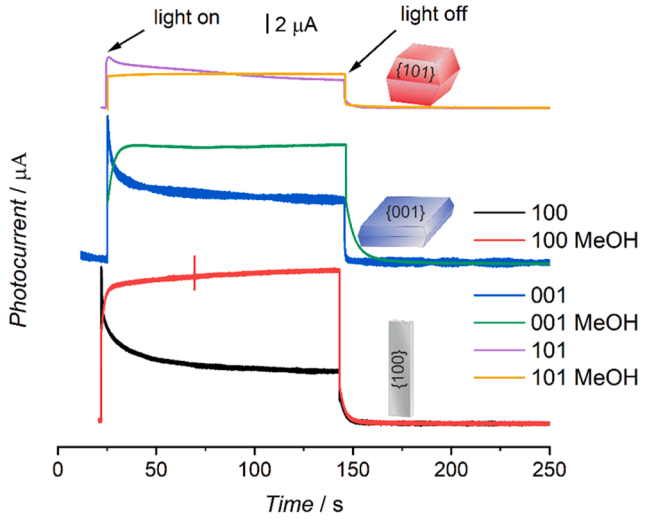

Fig. 4. Transient photocurrent response of electrodes made of various tailored TiO_2 crystals with and without methanol (5% w/w). LED 375 nm diode was the source of light, the applied potential was set at 1.0 V *vs.* RHE.

(Fig. 4) [43–45]. Due to the slow kinetics of water oxidation by photogenerated holes, a sharp maximum of photocurrent shortly after opening the shutter is followed by a continuous decay of photocurrent due to enhanced recombination of surface-accumulated holes with electrons, until a steady state is reached. In contrast, in the *presence* of methanol the recombination of photogenerated holes is supressed due to their fast reaction with methanol that is more readily oxidizable than water. As a result, photocurrents are stable and again their magnitude increases in the order **101** < **001** < **100**. Interestingly, the photocurrent even slowly increases during prolonged irradiation, which is most notable in the case of the **100** sample. This may be attributed to the continuously improving transport of photogenerated electrons to the underlying electrode. The electron transport in TiO_2 is typically understood in terms of trap states-assisted diffusion of electrons [45], and we assume that the increased population of the traps during prolonged irradiation and effective injection of electrons from hydroxymethyl radical intermediates (photocurrent doubling) may improve the transport properties and increase slightly the photocurrent. Another possible explanation for the slight increase of photocurrent during prolonged irradiation is the formation of formaldehyde upon partial methanol oxidation, whereby formaldehyde can be even easier oxidized, giving thus a higher photocurrent and a more pronounced photocurrent doubling effect.

Table 1
Current-voltage characteristics of PFC in the presence of studied electrodes. Experiments were done under polychromatic irradiation (AM 1.5G; 1.07 sun); 5% MeOH (w/w) in 0.1 M KOH.

	100	**101**	**001**
J_{sc}/mA/cm^2	0.496	0.150	0.182
V_{oc}/V	1.00	0.617	0.829
P_{MAX}/mW/cm^2	0.2	0.03	0.07
Efficiency/%	0.19	0.028	0.065
FF	0.21	0.32	0.46

3.3. Photocatalytic fuel cell performance

The photocatalytic fuel cell performance was tested by recording polarization curves in a two-electrode setup in electrolytes in equilibrium with air. In order to determine the optimal fuel concentration, measurements of J-V curves for various methanol concentrations (1%, 5%, 10%; w/w) at pH = 13 were performed (Fig. S2). A strong dependence of PFC performance on fuel concentration was revealed. For all studied photoanodes the highest power density was achieved for 5% (w/w) methanol. The maximum power densities of 0.2, 0.03 and 0.07 mW/cm^2 for the **100**, **101** and **001** TiO_2 materials, respectively, were determined (Table 1). Detailed data describing the main parameters of PFCs for different concentrations of methanol, including the short circuit photocurrent (J_{SC}), open circuit voltage (V_{OC}), efficiency (%) and fill factor (FF) are presented in Table S1. Taking into account these data, further PFCs tests were done at pH = 13 and the fuel concentration of 5% (w/w).

The next step was to test various alcohols as fuels. Simple alcohols are very cheap, since they are often side products of many industrial processes. Moreover, they can be produced from biomass. Performances of PFCs with methanol, ethanol, 2-propanol, *n*-butanol, *t*-butanol and glycerol as possible fuels were investigated. Corresponding polarization curves are presented in Fig. 5. For each studied electrode, the highest power density was observed for methanol as a fuel. Interestingly, in the case of photoanodes covered by **100** and **101** materials in the presence of *t*-butanol the worst PFC performances were recorded – measured power densities were lower than for a fuel-free system. In general, the simpler molecular structure of the alcohol, the better PFC performance. The maximum power density of 0.205 mW/cm^2 was recorded for the electrode covered by **100** material in the presence of methanol, with J_{SC} = 0.49 mA/cm^2 and V_{OC} = 1.00 V (Fig. 5a, Table S2a). This value is ~

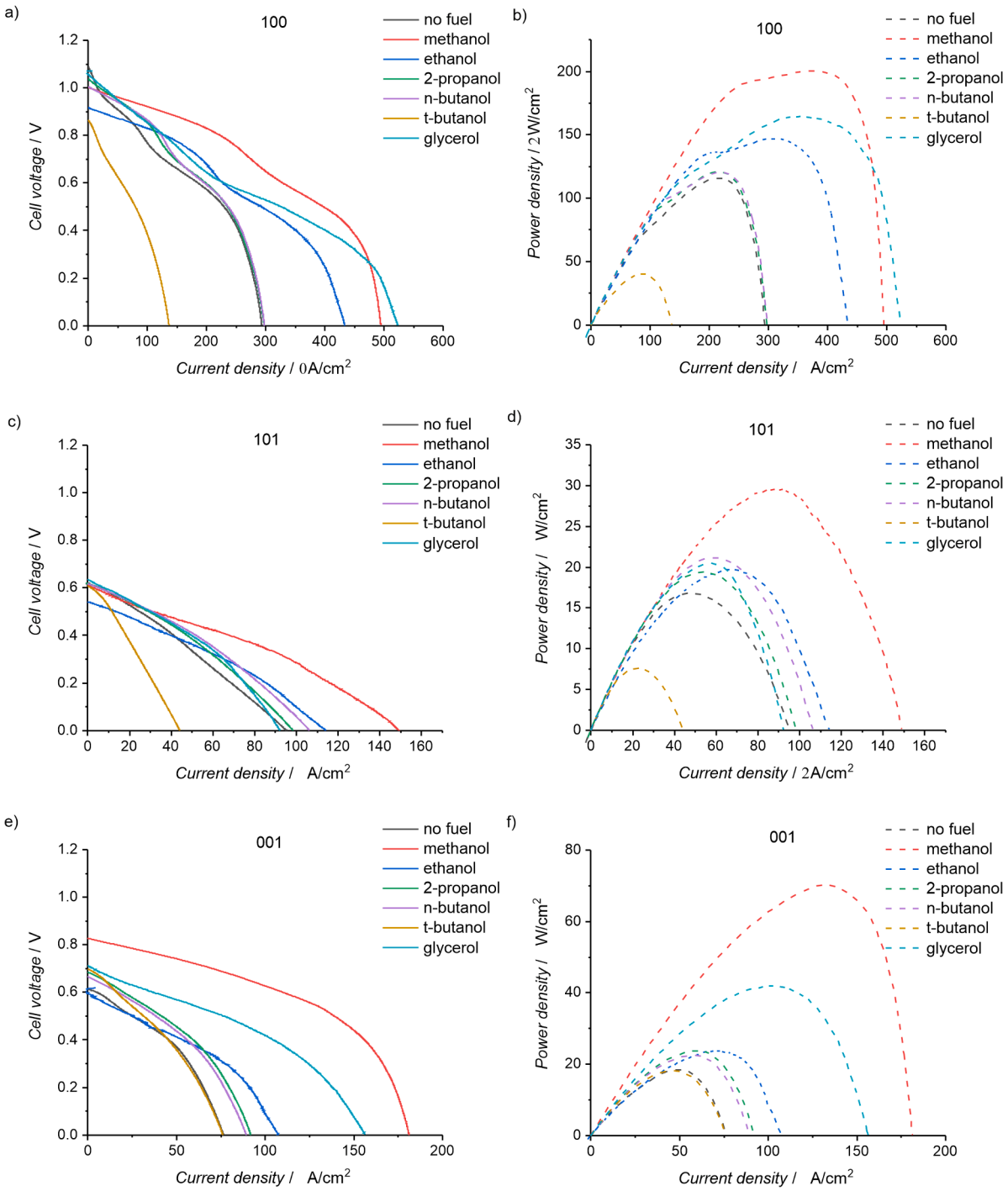

Fig. 5. Polarization curves and power densities for different fuels 5% (w/w) in 0.1 M KOH (pH = 13): a), b) belts (**100**), c), d) tetragonal truncated bipyramids (**101**), e), f) sheets (**001**). Experiments were done in two-electrode system under polychromatic irradiation (AM1.5G; 1.07 sun).

8% of the maximum power density of 2.54 mW/cm^2 for a hypothetical anatase photoanode, determined as the product of the maximum theoretical voltage of 1.186 V for methanol /O_2 fuel cell and maximum current density of 2.14 mA/cm^2 determined by the bandgap of 3.2 eV and the integration of an AM 1.5G (1 sun) spectrum down to 388 nm (assuming the photocurrent doubling effect). Furthermore, a good performance for glycerol and ethanol was observed (P_{MAX} = 0.165 and 0.147 mW/cm^2, respectively). No significant increase of the PFC power density for *n*-butanol and 2-propanol as fuels, compared to the fuel free system, was noticed (Fig. 5b, Table S2a). Only the electrode coated by **100** showed a non-linear relationship in the ohmic polarisation region. Kinks in polarisation curves reduce the fill factor value and hence the efficiency of tested systems.

In the case of the electrode covered by **101**, the maximum PFC power density of 0.030 mW/cm^2 was observed in the presence of methanol. J_{SC} and V_{OC} reached the levels of 0.150 mA/cm^2 and 0.617 V, respectively (Fig. 5c, Table S2a). In the case of ethanol, 2-propanol, *n*-butanol and glycerol used as a fuels, the performance of PFC was similar, slightly better compared to the system without any fuel (Fig. 5d, Table S2b). The lowest power density and the low difference between various fuels seem to result from the exposition of low active {1 0 1} crystal facets within the **101** material.

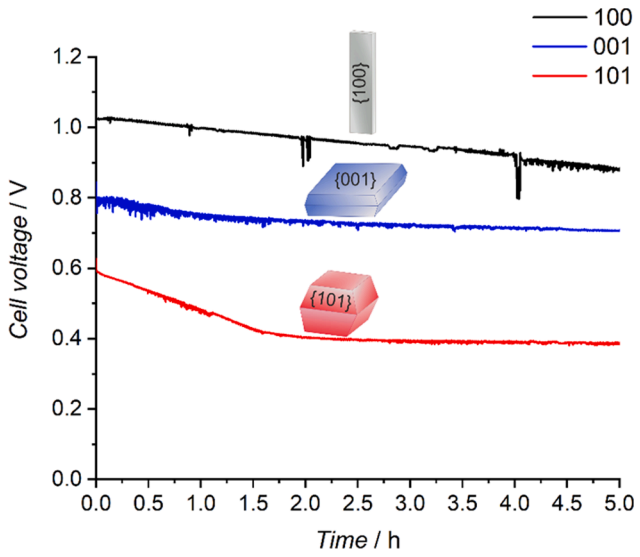

Fig. 6. Discharging performances of the PFC operation at a constant discharging current density of 20 μA/cm^2 in 0.1 M KOH with 5% (w/w) methanol. Experiments were done in two-electrode system under polychromatic irradiation (AM 1.5G; 1.07 sun).

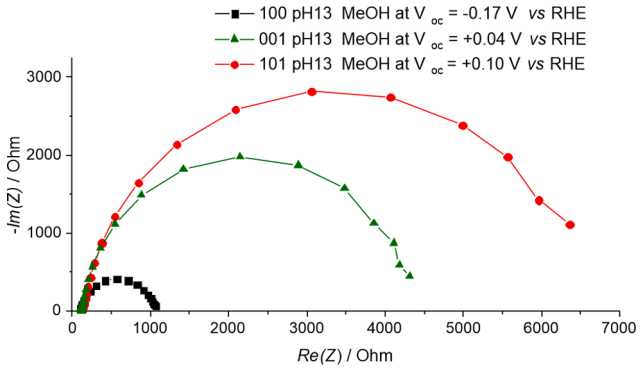

Fig. 7. Nyquist plot of the irradiated electrodes (AM 1.5G; 1.07 sun) at V_{OC} potential in the presence of methanol at pH = 13.

Similar to other materials, also for the **001** sample the maximum PFC power density of 0.070 mW/cm^2 was observed in the presence of methanol. J_{SC} and V_{OC} were found to be equal to 0.182 mA/cm^2 and 0.829 V, respectively (Fig. 5e, Table S2a). In the case of the electrode coated by **001**, a quite effective PFC performance for glycerol as a fuel (P_{MAX} = 0.0421 mW/cm^2) was observed. The strongly detrimental effect of *t*-butanol on photocurrent generation observed for **100** and **101** samples (Fig. 5f, Table S2c) was not observed in case of **001**, which might indicate a relatively better adsorption and/or oxidation of this compound at {0 0 1} facets. Yet, the photocurrents were in the range corresponding to experiments without any additional fuel.

A long term performance is another important feature of a fuel cell. Fig. 6 shows the PFCs performance for the studied photoanodes at a constant discharging current density of 20 μA/cm^2 in the alkaline electrolyte (pH = 13) for 5 h. An instability of the cell voltage for all tailored TiO_2 materials was noticed. In the case of the photoelectrode covered by **100**, the cell voltage decreased from *ca.* 1.03 to 0.88 V after 5 h of the experiment. For **001** material the cell voltage diminished from *ca.* 0.8 to 0.72 V after 3 h and remained constant to the end of experiment. Similarly, for **101** material, a decrease of the cell voltage from *ca.* 0.6 to 0.4 V after 2 h was observed.

3.4. Open-circuit photopotential and electrochemical impedance spectroscopy

Electrochemical impedance spectroscopy at open-circuit photopotential (V_{oc}) was applied to investigate the AC response of the photoelectrodes and in order to shed some light on the superior fuel cell efficiency of the **100** belts. Two observations are particularly noteworthy. Firstly, in the presence of methanol and under illumination, the open-circuit photopotentials recorded under identical conditions differ significantly for different materials: –0.17 V, +0.04 V, and +0.10 V *vs* RHE for **100**, **001**, **101**, respectively. Secondly, the Nyquist plots of the impedance response of all photoanodes measured at V_{oc} under light and in the presence of methanol exhibit single semicircles with radii increasing in the order **100** < **001** < **101**, *i.e.*, the size of the semicircle follows inversely the order of the open-circuit photopotentials (Fig. 7). In general, the open-circuit photopotential is determined by the *quasi*-Fermi level of electrons. It depends on the density of electrons accumulated in the material and on the position of the conduction band edge. While the former is the result of a complex interplay between the charge generation, transfer and recombination processes in the TiO_2 crystals, the latter depends on the net surface charge (*i.e.*, on the potential drop across the Helmholtz double layer) and might be, under irradiation, significantly influenced by the presence of surface states. In other words, one can assume that if, for example, the photogenerated holes do not react fast with species in the electrolyte but are trapped in the surface states, then the overall surface charge turns positive, leading to the shift of the conduction band edge to more positive electrode potentials, and – in turn – to less negative open-circuit photopotentials. Such effects are often referred to as "Fermi level pinning" or "unpinning of band edges". Based on these considerations, the fact that the **100** electrode exhibits the most negative V_{oc} under irradiation therefore clearly reflects the highest rate of methanol oxidation at **100**, as compared to **001** and **101**. Notably, if the measurements were performed in the *absence* of methanol (Fig. S3), the V_{oc} values were less negative and rather similar for all materials, which again highlights the important role of methanol oxidation for efficient extraction of the holes from the crystals, thereby promoting negative charge accumulation and avoiding the undesired unpinning of band edges. The fact that there is a clear correlation between the photoelectrocatalytic performance (**1 0 0**> **001** > **101**; Figs. 4 and 6) and the size of semicircles in the Nyquist plots (**100** < **001** < **1 0 1**) recorded at open-circuit potentials (Fig. 7) therefore suggests that the impedance response is strongly influenced by the rate of methanol oxidation by photogenerated holes, rather than dominated solely by different charge transport properties (*i.e.*, conductivity) due to different density of electrons in the conduction band and the trap states under the conduction band edge. In this context, we note that in the *absence* of methanol, virtually identical Nyquist plots (Fig. S3) were recorded for all samples under light at comparable V_{oc} values, suggesting that, in the absence of methanol, the charge transfer and charge transport in the bulk of **001** and **101** crystals are similar. From these results, we conclude that the single semicircles (corresponding to single RC time constants) recorded in the presence of methanol (Fig. 7) are mainly influenced by the efficiency of the charge transfer at the TiO_2/electrolyte interface. The RC time constants were determined from the Bode plots (Fig. S4) and the estimated values increase from 87 to 175 and 188 ms for **100**, **001** and **101** crystals, respectively. Therefore, the superior methanol oxidation at the {1 0 0} facets of TiO_2 belts most likely arises from the faster charge transfer of photogenerated holes to methanol molecules. Herein, we note that the {1 0 0} facets predominating in our **100** belts are neither observed in natural anatase crystals, nor in other materials studied within this work. In contrast, the tetragonal truncated bipyramids crystals (**1 0 1**) exhibited the largest semicircle in the Nyquist plots, in line with the poorest photoelectrocatalytic performance of the **101** material. In our previous studies we found that home-made, well-defined tailored crystals contain much less surface defects compared to the commercial materials [23,46], and deep surface states are present

only in the case of **101** materials [23]. In case of a simple, nonselective alcohol oxidation (possibly involving both direct oxidation by holes and by surface bound $HO^{\bullet}$ radicals) it seems that such deep surface electronic states can decrease the reaction efficiency by acting as trap states for holes, increasing thus the recombination and inducing undesired shifts of the band edges.

4. Conclusions

We have studied, for the first time, the PFC performance of photoanodes based on anatase crystals of various shapes – tetragonal truncated bipyramids, sheets and belts, which are characterized by different predominantly exposed facets: {101}, {001}, and {100}, respectively. We show that photoanodes based on belt-shaped crystals dominated by {100} facets exhibit superior performance reaching the maximum power density of 0.205 mW/cm^2 (under ~1 sun), which is *ca.* 8% of the theoretical limit. Based on the differences in open-circuit photopotential and impedance response of the different photoanodes, we conclude that the superior performance of the belt-like material dominated by {100} facets is related to faster transfer of photogenerated holes to methanol molecules, avoiding thus the undesired surface trapping and Fermi level pinning effects that are the most likely cause of poorer performance of materials dominated by {101} and {001} facets. In this context, we point out that the best performing {100} facets are not observed in natural anatase crystals, which highlights the importance of advanced crystal engineering and control over the surface catalytic properties of TiO_2 materials for PFCs and other light-driven devices in which high rate of alcohol photooxidation is mandatory.

CRediT authorship contribution statement

Paweł Mikrut: Conceptualization, Methodology, Investigation, Writing – original draft, Project administration, Funding acquisition. **Dariusz Mitoraj:** Formal analysis, Investigation, Writing – original draft, Supervision, Project administration. **Radim Beranek:** Formal analysis, Writing – original draft. **Wojciech Macyk:** Conceptualization, Supervision, Writing – original draft.

Declaration of Competing Interest

The authors declare that they have no known competing financial interests or personal relationships that could have appeared to influence the work reported in this paper.

Acknowledgements

The work was supported by the National Science Centre, Poland (NCN) within the Preludium 17 project (2019/33/N/ST4/01572). D.M. and R.B. acknowledge the support by the Deutsche Forschungsgemeinschaft (DFG, German Research Foundation) – projects BE 5102/5-1 and 364549901 – TRR 234 CataLight [Project B6].

Appendix A. Supplementary material

Supplementary data to this article can be found online at https://doi.org/10.1016/j.apsusc.2021.150662.

References

[1] M. Alias, S. Kamarudin, A. Zainoodin, M. Masdar, Active direct methanol fuel cell: An overview, Int. J. Hydrog. Energy (2020).
[2] K. Drew, G. Girishkumar, K. Vinodgopal, P.V. Kamat, Boosting fuel cell performance with a semiconductor photocatalyst: TiO_2/Pt– Ru hybrid catalyst for methanol oxidation, J. Phys. Chem. B 109 (2005) 11851–11857.
[3] M. Antoniadou, P. Lianos, Production of electricity by photoelectrochemical oxidation of ethanol in a PhotoFuelCell, App. Catal. B: Environ. 99 (2010) 307–313.
[4] M. Kaneko, J. Nemoto, H. Ueno, N. Gokan, K. Ohnuki, M. Horikawa, R. Saito, T. Shibata, Photoelectrochemical reaction of biomass and bio-related compounds with nanoporous TiO_2 film photoanode and O_2-reducing cathode, Electrochem. Commun. 8 (2006) 336–340.
[5] M. Li, Y. Liu, L. Dong, C. Shen, F. Li, M. Huang, C. Ma, B. Yang, X. An, W. Sand, Recent advances on photocatalytic fuel cell for environmental applications-The marriage of photocatalysis and fuel cells, Sci. Total Environ. 668 (2019) 966–978.
[6] B. Deng, S. Fu, Y. Zhang, Y. Wang, D. Ma, S. Dong, Simultaneous pollutant degradation and power generation in visible-light responsive photocatalytic fuel cell with an Ag-TiO_2 loaded photoanode, Nano-Struct. Nano-Objects 15 (2018) 167–172.
[7] L. Li, G. Wang, R. Chen, X. Zhu, H. Wang, Q. Liao, Y. Yu, Optofluidics based micro-photocatalytic fuel cell for efficient wastewater treatment and electricity generation, Lab Chip 14 (2014) 3368–3375.
[8] Y. He, Y. Zhang, L. Li, W. Shen, J. Li, An efficient optofluidic photocatalytic fuel cell with dual-photoelectrode for electricity generation from wastewater treatment, J. Solid State Chem. 293 (2020) 121780.
[9] M. Kaneko, N. Gokan, N. Katakura, Y. Takei, M. Hoshino, Artificial photochemical nitrogen cycle to produce nitrogen and hydrogen from ammonia by platinized TiO_2 and its application to a photofuel cell, Chem. Commun. (2005) 1625–1627.
[10] M. Xia, R. Chen, X. Zhu, Q. Liao, L. An, Z. Wang, X. He, L. Jiao, A micro photocatalytic fuel cell with an air-breathing, membraneless and monolithic design, Sci. Bull. 61 (2016) 1699–1710.
[11] Y. Ogura, S. Okamoto, T. Itoi, Y. Fujishima, Y. Yoshida, Y. Izumi, A photofuel cell comprising titanium oxide and silver (I/0) photocatalysts for use of acidic water as a fuel, Chem. Commun. 50 (2014) 3067–3070.
[12] J. Georgieva, E. Valova, I. Mintsouli, S. Sotiropoulos, D. Tatchev, S. Armyanov, A. Hubin, J. Dille, A. Hoell, V. Raghuwanshi, Pt (Ni) electrocatalysts for methanol oxidation prepared by galvanic replacement on TiO_2 and TiO_2–C powder supports, J. Electroanal. Chem. 754 (2015) 65–74.
[13] Y. Ito, T. Takeuchi, T. Tsujiguchi, M.A. Abdelkareem, N. Nakagawa, Ultrahigh methanol electro-oxidation activity of PtRu nanoparticles prepared on TiO_2-embedded carbon nanofiber support, J. Power Sources 242 (2013) 280–288.
[14] N. Li, S. Tang, Y. Rao, J. Qi, Q. Zhang, D. Yuan, Peroxymonosulfate enhanced antibiotic removal and synchronous electricity generation in a photocatalytic fuel cell, Electrochim. Acta 298 (2019) 59–69.
[15] B. Wang, H. Zhang, X.-Y. Lu, J. Xuan, M.K. Leung, Solar photocatalytic fuel cell using CdS–TiO_2 photoanode and air-breathing cathode for wastewater treatment and simultaneous electricity production, Chem. Eng. J. 253 (2014) 174–182.
[16] Q. Liao, L. Li, R. Chen, X. Zhu, H. Wang, D. Ye, X. Cheng, M. Zhang, Y. Zhou, Respective electrode potential characteristics of photocatalytic fuel cell with visible-light responsive photoanode and air-breathing cathode, Int. J. Hydrog. Energy 40 (2015) 16547–16555.
[17] Y. Wang, Y. Lan, D. Bu, B. Qian, Y. Wang, B. Wang, Q. Wu, S. Li, Y. Zhang, X.-M. Song, A study on tandem photoanode and photocathode for photocatalytic formaldehyde fuel cell, Electrochim. Acta 352 (2020) 136476.
[18] Q. Zeng, S. Chang, A. Beyhaqi, S. Lian, H. Xu, J. Xie, F. Guo, M. Wang, C. Hu, Efficient solar hydrogen production coupled with organics degradation by a hybrid tandem photocatalytic fuel cell using a silicon-doped TiO_2 nanorod array with enhanced electronic properties, J. Hazard. Mater. 394 (2020) 121425.
[19] X. Li, G. Wang, L. Jing, W. Ni, H. Yan, C. Chen, Y.-M. Yan, A photoelectrochemical methanol fuel cell based on aligned TiO_2 nanorods decorated graphene photoanode, Chem. Commun. 52 (2016) 2533–2536.
[20] X. Han, Q. Kuang, M. Jin, Z. Xie, L. Zheng, Synthesis of titania nanosheets with a high percentage of exposed (001) facets and related photocatalytic properties, J. Am. Chem. Soc. 131 (2009) 3152–3153.
[21] J. Pan, G. Liu, G.Q. Lu, H.M. Cheng, On the true photoreactivity order of 001}, {010}, and {101 facets of anatase TiO_2 crystals, Angew. Chem. Int. Ed. 50 (2011) 2133–2137.
[22] F. Pellegrino, F. Sordello, L. Mino, C. Minero, V.-D. Hodoroaba, G. Martra, V. Maurino, Formic acid photoreforming for hydrogen production on shape-controlled anatase TiO_2 nanoparticles: Assessment of the role of fluorides,{101}/{001} surfaces ratio, and platinization, ACS Catal. 9 (2019) 6692–6697.
[23] P. Mikrut, M. Kobielusz, W. Macyk, Spectroelectrochemical characterization of euhedral anatase TiO_2 crystals – implications for photoelectrochemical and photocatalytic properties of (001)(100) and (101) facets, Electrochim. Acta 310 (2019) 256–265.
[24] A.-Y. Zhang, W.-Y. Wang, J.-J. Chen, C. Liu, Q.-X. Li, X. Zhang, W.-W. Li, Y. Si, H.-Q. Yu, Epitaxial facet junctions on TiO_2 single crystals for efficient photocatalytic water splitting, Energy Environ. Sci. 11 (2018) 1444–1448.
[25] S. Kashiwaya, T. Toupance, A. Klein, W. Jaegermann, Fermi level positions and induced band bending at single crystalline anatase (101) and (001) surfaces: origin of the enhanced photocatalytic activity of facet engineered crystals, Adv. Energy Mater. 8 (2018) 1802195.
[26] L. Guan, X. Chen, Photoexcited charge transport and accumulation in anatase TiO_2, ACS Appl. Energy Mater. 1 (2018) 4313–4320.
[27] K. Kobayashi, M. Takashima, M. Takase, B. Ohtani, Mechanistic study on facet-dependent deposition of metal nanoparticles on decahedral-shaped anatase titania photocatalyst particles, Catalysts 8 (2018) 542.
[28] K. Wenderich, A. Klaassen, I. Siretanu, F. Mugele, G. Mul, Sorption-Determined Deposition of Platinum on Well-Defined Platelike WO_3, Angew. Chem. Int. Ed. 53 (2014) 12476–12479.
[29] C. Adler, D. Mitoraj, I. Krivtsov, R. Beranek, On the importance of catalysis in photocatalysis: Triggering of photocatalysis at well-defined anatase TiO_2 crystals through facet-specific deposition of oxygen reduction cocatalyst, J. Chem. Phys. 152 (2020).

[30] X.-Q. Gong, A. Selloni, Reactivity of anatase TiO_2 nanoparticles: the role of the minority (001) surface, J. Phys. Chem. B 109 (2005) 19560–19562.
[31] Q. Wu, M. Liu, Z. Wu, Y. Li, L. Piao, Is photooxidation activity of 001 facets truly lower than that of 101 facets for anatase TiO_2 crystals? J. Phys. Chem. C 116 (2012) 26800–26804.
[32] F.H. Tian, X. Wang, W. Zhao, L. Zhao, T. Chu, S. Yu, Adsorption of 2-propanol on anatase TiO_2 (101) and (001) surfaces: A density functional theory study, Surf. Sci. 616 (2013) 76–84.
[33] M. Setvin, X. Shi, J. Hulva, T. Simschitz, G.S. Parkinson, M. Schmid, C. Di Valentin, A. Selloni, U. Diebold, Methanol on anatase TiO_2 (101): Mechanistic insights into photocatalysis, ACS Catal. 7 (2017) 7081–7091.
[34] H. Tang, Z. Cheng, S. Dong, X. Cui, H. Feng, X. Ma, B. Luo, A. Zhao, J. Zhao, B. Wang, Understanding the Intrinsic Chemical Activity of Anatase TiO_2(001)-(1×4) Surface, J. Phys. Chem. C 121 (2017) 1272–1282.
[35] M. Khalil, F. Naumi, U. Pratomo, T.A. Ivandini, G.T. Kadja, J.Y. Mulyana, Coexposed TiO_2 001 and 101 facets in $TiO_2/BiVO_4$ photoanodes for an enhanced photocatalytic fuel cell, Appl. Surf. Sci. 542 (2021) 148746.
[36] J. Wang, Z. Bian, J. Zhu, H. Li, Ordered mesoporous TiO_2 with exposed 001 facets and enhanced activity in photocatalytic selective oxidation of alcohols, J. Mater. Chem. 1 (2013) 1296–1302.
[37] X. Pan, N. Zhang, X. Fu, Y.-J. Xu, Selective oxidation of benzyl alcohol over TiO_2 nanosheets with exposed 001 facets: Catalyst deactivation and regeneration, Appl. Catal. A 453 (2013) 181–187.
[38] R. Vadakkekara, A.K. Biswas, T. Sahoo, P. Pal, B. Ganguly, S.C. Ghosh, A.B. Panda, Visible-light-induced efficient selective oxidation of nonactivated alcohols over {001}-faceted TiO_2 with molecular oxygen, Asian J. Chem. 11 (2016) 3084–3089.
[39] H. Rensmo, H. Lindström, S. Södergren, A.-K. Willstedt, A. Solbrand, A. Hagfeldt, S.-E. Lindquist, Photocurrent losses in Nanocrystalline/Nanoporous TiO_2 electrodes due to electrochemically active species in the electrolyte, J. Electrochem. Soc. 143 (1996) 3173.
[40] A. Hagfeldt, U. Björkstén, S.-E. Lindquist, Photoelectrochemical studies of colloidal TiO_2-films: the charge separation process studied by means of action spectra in the UV region, Sol. Energy Mater. Sol. Cells 27 (1992) 293–304.
[41] T. Berger, D. Monllor-Satoca, M. Jankulovska, T. Lana-Villarreal, R. Gómez, The electrochemistry of nanostructured titanium dioxide electrodes, Chem. Phys. Chem. 13 (2012) 2824–2875.
[42] E. Kalamaras, P. Lianos, Current Doubling effect revisited: Current multiplication in a PhotoFuelCell, J. Electroanal. Chem. 751 (2015) 37–42.
[43] M. Bledowski, L. Wang, S. Neubert, D. Mitoraj, R. Beranek, Improving the performance of hybrid photoanodes for water splitting by photodeposition of iridium oxide nanoparticles, J. Phys. Chem. C 118 (2014) 18951–18961.
[44] L. Wang, M. Bledowski, A. Ramakrishnan, D. König, A. Ludwig, R. Beranek, Dynamics of photogenerated holes in TiO_2-polyheptazine hybrid photoanodes for visible light-driven water splitting, J. Electrochem. Soc. 159 (2012) H616.
[45] L.M. Peter, Dynamic aspects of semiconductor photoelectrochemistry, Chem. Rev. 90 (1990) 753–769.
[46] M. Kobielusz, K. Pilarczyk, E. Święţek, K. Szaciłowski, W. Macyk, Spectroelectrochemical analysis of TiO_2 electronic states–Implications for the photocatalytic activity of anatase and rutile, Catal. Today 309 (2018) 35–42.